


# Antibacterial Property and Mechanisms of Au@Ag Core-Shell Nanoparticles with Near-Infrared Absorption Against *E. faecalis* Infection of Dentin

Yaxu Feng\*, Qing Sun\*, Pei Liu , Wei Fan , Bing Fan

The State Key Laboratory of Oral & Maxillofacial Reconstruction and Regeneration, Key Laboratory of Oral Biomedicine Ministry of Education, Hubei Key Laboratory of Stomatology, School & Hospital of Stomatology, Wuhan University, Wuhan, People's Republic of China

\*These authors contributed equally to this work

Correspondence: Wei Fan; Bing Fan, Email weifan@whu.edu.cn; bingfan@whu.edu.cn

**Background:** *Enterococcus faecalis* (*E. faecalis*) is one of the main pathogens responsible for refractory root canal infections in the teeth and shows resistance against various antibacterial managements. Effective control of *E. faecalis* infection is a prerequisite for successful treatment of refractory apical periodontitis. This study aimed to analyze the antibacterial activity and mechanisms of Au@Ag nanoparticles (NPs) combined with photothermal therapy (PTT) against the original and Ag<sup>+</sup>-resistant *E. faecalis*.

**Methods:** Au@AgNPs with optimal shell thicknesses were synthesized and characterized. The antibacterial activity of Au@AgNPs with PTT against the original or Ag<sup>+</sup>-resistant *E. faecalis* was evaluated, and the antibiofilm activity was tested on *E. faecalis* biofilm on the dentin of teeth. The potential antibacterial mechanisms of Au@AgNPs combined with PTT against *E. faecalis* have also been studied. Moreover, its influence on dentin microhardness and cytotoxicity was assessed.

**Results:** This study revealed that Au@AgNPs combined with PTT showed enhanced antibacterial and antibiofilm effects, no negative effects on dentin microhardness, and low cytotoxicity toward human periodontal ligament cells (hPDLs). Moreover, Au@AgNPs combined with PTT effectively inhibited the growth of Ag<sup>+</sup>-resistant *E. faecalis*. Its antibacterial effects may be exerted through the release of silver ions (Ag<sup>+</sup>), destruction of the cell membrane, production of reactive oxygen species (ROS) and inhibition of adenosine triphosphate (ATP) production. Hyperthermia generated by Au@AgNPs with PTT reduced membrane fluidity and enhanced Ag<sup>+</sup> sensitivity by downregulating *fabF* expression. The upregulated expression of heat shock genes demonstrated that the Ag<sup>+</sup> released from Au@AgNPs compromised the heat adaptation of *E. faecalis*.

**Conclusion:** PTT significantly enhanced Ag<sup>+</sup> sensitivity of the original and Ag<sup>+</sup>-resistant *E. faecalis*. Au@AgNPs combined with PTT may have the potential to be developed as a new antibacterial agent to control *E. faecalis* infections in teeth.

**Keywords:** Au@AgNPs, resistance, photothermal therapy, antibacterial, silver ions, *E. faecalis*

## Introduction

Refractory apical periodontitis (RAP) is chronic apical infection of teeth that persists after primary root canal therapy.<sup>1</sup> *Enterococcus faecalis* (*E. faecalis*) is the one of the main pathogens isolated from root canals of teeth with RAP.<sup>2-4</sup> It has been confirmed that *E. faecalis* could tolerate antibiotics and survive in various harsh environments and disinfection procedures.<sup>5,6</sup> In addition, *E. faecalis* can form biofilm in complicated root canal anatomy and dentinal tubules, thus being difficult to eliminate.<sup>7</sup>

As many bacteria can develop antibiotic resistance after repeated exposure to antibiotics, metal-based nanoparticles have been used as alternatives to antibiotics against pathogens.<sup>8</sup> Silver nanoparticles (AgNPs) have been reported to be effective in the control of root canal infections.<sup>9,10</sup> Wu et al reported that the antibacterial efficacy of AgNPs against *E. faecalis* was positively correlated with exposure time.<sup>11</sup> Although antimicrobial activity is directly related to the amount of Ag<sup>+</sup> released, the cytotoxicity also increases with the increase in Ag<sup>+</sup> concentration.<sup>12,13</sup> In addition, AgNPs are easily oxidized.<sup>14,15</sup> Recent

studies have reported that long-term exposure to  $\text{Ag}^+$  could induce Ag-resistant *E. faecalis*.<sup>16,17</sup> Hence, optimizing the structure of AgNPs to reduce silver resistance is of great significance in application.

Gold nanoparticles is one of the ideal therapeutic materials because of its easy preparation, good biocompatibility, high surface area and ability to conjugated to other materials, but it showed limited antibacterial property.<sup>14,18</sup> Bimetallic nanoparticles have been found to have stronger antibacterial property than monometallic versions due to the synergistic effect between the metals.<sup>15</sup> Previous studies reported that Au@Ag core-shell nanoparticles (NPs) showed excellent antibacterial effect through disrupting the cell membrane and generating reactive oxygen species (ROS).<sup>14,19</sup> Meanwhile, bimetallic Au@AgNPs could also be efficient against multidrug-resistant (MDR) bacteria.<sup>15</sup> In addition, Au-based nanomaterial is one of the most promising photothermal therapy (PTT) agents, as they can be easily fabricated in different shapes and sizes which greatly affected optical properties.<sup>20</sup> Despite this, gold nanospheres less than 50 nm show limited absorption of near-infrared (NIR) spectrum.<sup>18</sup> Yuan et al pointed that a new localized surface plasmon resonance (LSPR) band appeared in the longer wavelength in extinction spectra at the presence of NaCl, which indicated the formation of small diameter Au@AgNPs aggregates.<sup>21</sup> Therefore, it could be envisioned that the aggregation formed by small diameter Au@AgNPs in phosphate buffer saline (PBS) medium may enhance photothermal activity, which irreversibly cause bacterial death by generated high temperatures.<sup>22</sup> However, the antimicrobial properties of Au@AgNPs combined with PTT against original or  $\text{Ag}^+$ -resistant *E. faecalis* has not yet been studied.

With Ag-based materials applied in various fields, the emergence of silver-resistant strains would pose a serious threat to human health.<sup>12</sup> To be against silver-resistant bacteria, some researchers have tried to enhance antibacterial effects by combining  $\text{Ag}^+$ /AgNPs with other medicines or improving AgNPs,<sup>23,24</sup> but studies on antibacterial efficacy against  $\text{Ag}^+$ -resistant *E. faecalis* are still lacking. Therefore, the present study developed Au@Ag core-shell nanoparticles with an optimum Ag shell thickness that possess a synergistic effect of photothermal properties and antibacterial activity. Furthermore, such antibacterial agents can be effective against  $\text{Ag}^+$ -resistant *E. faecalis*. Based on this, the potential antibacterial mechanisms of Au@AgNPs combined with PTT were further investigated.

## Materials and Methods

### Materials

Gold chloride trihydrate ( $\text{HAuCl}_4 \cdot 3\text{H}_2\text{O}$ ) and PVP (MW=10000) were purchased from Aladdin Biotechnology Co. Ltd. (Shanghai, China). Sodium citrate tribasic dihydrate was obtained from Sigma-Aldrich (St. Louis, MO, USA). Sodium hydroxide (NaOH), l-ascorbic acid (AA) and silver nitrate ( $\text{AgNO}_3$ ) were purchased from Sinopharm Chemical Reagent Co. Ltd. (Shanghai, China). All chemicals were of analytical grade, and no further purification was required. Milli-Q water with a resistivity of 18.2 M $\Omega$  was used throughout material synthesis.

### Synthesis of AuNPs

$\text{HAuCl}_4 \cdot 3\text{H}_2\text{O}$  solution (0.29 M, 100  $\mu\text{L}$ ) was added to a 250 mL round-bottom flask with preboiled ultrapure water (100 mL) and boiled for 5 min. Sodium citrate solution (38 mM, 2.4 mL) was added, and the mixture was boiled and stirred for 30 min. The resulting wine-red AuNPs solution was cooled at room temperature before further use.

### Synthesis of Au@AgNPs

PVP solution (1%, 10 mL) was added to the AuNPs solution dropwise and stirred for 10 min. The prepared  $\text{AgNO}_3$  solution (1 M, 200  $\mu\text{L}$ ) was added dropwise and stirred for 5 min. Subsequently, the AA solution (1 M, 150  $\mu\text{L}$ ) was added rapidly and stirred for 2 min, followed by the addition of NaOH solution (1 M, 400  $\mu\text{L}$ ) and continued stirring for 2 h until the color of the solution turned yellow-brown and stable. By fine-tuning the amount of the  $\text{AgNO}_3$  solution, Ag shells of Au@AgNPs with different thicknesses were synthesized.

After the completion of the reaction, the precipitate was washed and collected by centrifugation at 12,000 rpm for 20 min. Since the final product is a colloid, it's recommended that the precipitate be washed gently to avoid product loss. The final products were stored at 4°C in the dark until further characterization and application.

## Measurement and Characterization

Dynamic light scattering (DLS) and zeta potential measurements were performed using a nanoparticle size potentiometer (Zetasizer Nano ZSP; Malvern, Malvern, UK). Ultraviolet-visible-near-infrared (UV-vis-NIR) spectra of the NPs were recorded using a UV-spectrophotometer (UV-2700i, Shimadzu, Kyoto, Japan). The size and morphology of the NPs were examined using transmission electron microscopy (TEM; JEM-2100, JEOL, Tokyo, Japan). The elemental composition and distribution mapping were determined using TEM (JEM-F200, JEOL, Tokyo, Japan) equipped with a super spectrometer (JED-2300T). The crystal structure was determined by X-ray diffraction (XRD; XPert Pro, PANalytical, Almoro, Netherlands). The temperature of the NPs solution was measured using a thermocouple connected to a digital thermometer (LIHUADA, Shenzhen, China). Thermal images were recorded using an IR thermographic camera (FOTRIC225, Shanghai Thermal Image Electromechanical Technology Co. Ltd, Shanghai, China). In brief, before thermal images were recorded, Au@AgNPs (100, 200, 300, and 400 µg/mL) were injected into the cleaned and shaped root canal of human premolars to the level of the cemento-enamel junction using a 30-gauge needle and then irradiated by an 808 nm laser for 10 min.

## Silver Ions Release Profile

The release of Ag<sup>+</sup> from the Au@AgNPs with or without NIR irradiation in PBS was determined. Au@AgNPs solutions of the same concentration (200 µg/mL) were gently shaken at 37 °C. At different time points (10 min, 24, 72, and 120 h), the filtrate containing Ag<sup>+</sup> was collected by ultrafiltration of the Au@AgNPs suspension using Amicon® Ultra-0.5, centrifugal filter units with a cut-off size of 3 kDa (Merck Millipore, Darmstadt, Germany) at 15,000 g for 30 min.<sup>25,26</sup> The amount of released Ag<sup>+</sup> was analyzed by inductively coupled plasma mass spectrometry (ICP-MS, PQ-MS, Analytik Jena AG, Jena, Germany).

## Antimicrobial Effects Against Planktonic Original and Ag<sup>+</sup>-Resistant *E. faecalis*

### Antimicrobial Effects Against Original *E. faecalis*

The colony-forming units (CFUs) counting method was used to examine the antibacterial activity of the Au@AgNPs with or without NIR irradiation. *E. faecalis* (ATCC 29212, ATCC, Manassas, VA, USA) suspension of 1×10<sup>4</sup> CFUs/mL was incubated with Au@AgNPs solution at different concentrations (50, 100, 150, 200, 250, and 300 µg/mL) for 10 min in the presence or absence of irradiation with an 808 nm laser (1W/cm<sup>2</sup>). *E. faecalis* suspension treated with PBS without NIR was used as blank control and *E. faecalis* suspension incubated with 2% CHX or 2.5% NaClO was used as positive control. Subsequently, 10 µL of the inoculum from each group (n=6) was inoculated on a brain heart infusion (BHI) broth agar plate and incubated for another 24 h at 37°C anaerobically. Finally, the relative viability of *E. faecalis* was calculated using the following formula:

$$\text{Relative bacterial viability (\%)} = \text{CFUs of each group} / \text{Average CFUs of all blank control groups} \times 100\%.$$

In addition, *E. faecalis* suspension (1 × 10<sup>4</sup> CFUs/mL) was incubated with Au@AgNPs solution at different concentrations (50, 100, 150, 200, 250, and 300 µg/mL) for 10 min with or without NIR irradiation. At different time points (2, 4, and 6 h), 10 µL of the inoculum from each group (n=4) was inoculated on a BHI agar plate and incubated for another 24 h at 37°C anaerobically. Finally, the CFUs of *E. faecalis* were counted.

### Establishment of Ag<sup>+</sup>-Resistant *E. faecalis*

The minimal inhibitory concentration (MIC) of AgNO<sub>3</sub> against *E. faecalis* (1×10<sup>5</sup> CFUs/mL) was determined using the serial dilution method (ranging from 16 to 512 µg/mL). Ag<sup>+</sup>-resistant *E. faecalis* were selected by continuous exposure to AgNO<sub>3</sub>. Briefly, *E. faecalis* was cultured to 10<sup>9</sup> CFUs/mL, and the bacterial suspension was co-cultured with fresh BHI containing AgNO<sub>3</sub> (1/4MIC) at a ratio of 1:100 for 24 h and recorded as passage 1(P1). Then, overnight co-cultured bacteria (P1) were co-cultured again with fresh BHI containing AgNO<sub>3</sub> (1/4MIC) at a ratio of 1:100 for another 24 h and recorded as P2. Bacteria were co-cultured at the same AgNO<sub>3</sub> concentration and inoculated onto a BHI agar plate every four passages. After each inoculation, the AgNO<sub>3</sub> concentration was adjusted based on the turbidity of the co-culture liquid. This procedure was repeated 21 times.

Different concentrations of  $\text{AgNO}_3$  (1/2MIC, 1MIC, 2MIC) were co-cultured with the original or  $\text{Ag}^+$ -resistant *E. faecalis* ( $10^7$  CFUs/mL and  $10^8$  CFUs/mL) for 24 h, and then the optical density (OD) at 600 nm was measured using a microplate reader (Synergy H1, BioTek, Vermont, USA) to verify the increased  $\text{Ag}^+$ -resistance of *E. faecalis*. The experiment was repeated in triplicate.

### Antimicrobial Effects Against $\text{Ag}^+$ -Resistant *E. faecalis*

An  $\text{Ag}^+$ -resistant *E. faecalis* suspension ( $1 \times 10^4$  CFUs/mL) was incubated with Au@AgNPs at different concentrations (50, 100, 150, 200, 250, and 300  $\mu\text{g}/\text{mL}$ ) for 10 min in the presence or absence of irradiation with an 808 nm laser (1W/ $\text{cm}^2$ ). An  $\text{Ag}^+$ -resistant *E. faecalis* suspension treated with PBS without NIR irradiation was used as a blank control. Subsequently, 10  $\mu\text{L}$  of the inoculum from each group ( $n=6$ ) was inoculated onto a BHI agar plate and incubated for another 24 h at 37 °C anaerobically. Finally, the relative bacterial viability of  $\text{Ag}^+$ -resistant *E. faecalis* was calculated, as described in the section of antimicrobial effects against original *E. faecalis*.

Based on the  $\text{Ag}^+$  concentration released from Au@AgNPs under NIR irradiation for 10 min,  $\text{AgNO}_3$  with the same concentration of  $\text{Ag}^+$  was used as positive control to compare the antibacterial efficacy against  $\text{Ag}^+$ -resistant *E. faecalis*. Briefly, *E. faecalis* suspension of  $1 \times 10^4$  CFUs/mL was treated with Au@AgNPs with NIR or  $\text{AgNO}_3$  for 10 min. Subsequently, 10  $\mu\text{L}$  of the inoculum from each group ( $n=6$ ) was inoculated onto a BHI agar plate and incubated for another 24 h at 37°C anaerobically. Finally, the CFUs of  $\text{Ag}^+$ -resistant *E. faecalis* were counted.

### Antibiofilm Effects Against *E. faecalis* Biofilm on Dentin

Dentin slices ( $4 \times 4 \times 1$  mm) were prepared from extracted caries-free wisdom teeth. After being polished, all dentin slices were cleaned by ultrasonic washing successively in ddH<sub>2</sub>O (2 min), 5.25% NaClO (4 min), ddH<sub>2</sub>O (1 min), 17% EDTA (4 min), and ddH<sub>2</sub>O (1 min). The dentin slices were autoclaved at 121°C for 20 min in ddH<sub>2</sub>O. Sterilized dentin slices were soaked in 2 mL of *E. faecalis* suspension ( $10^8$  CFUs/mL) and incubated in anaerobic environment at 37 °C for 28 days. Fresh BHI broth was replaced every second day. The dentin slices were rinsed with PBS. Subsequently, the dentin slice was immersed in Au@AgNPs solution (400, 500, and 600  $\mu\text{g}/\text{mL}$ ) with irradiation with an 808 nm laser for 10 min and then incubated for another 10 min. The dentin slice immersed in PBS was used as blank control, and 2% CHX or 2.5% NaClO was used as positive control. Finally, dentin slices were washed again with PBS, and field emission scanning electron microscopy (FE-SEM, Zeiss GeminiSEM 500, Carl Zeiss AG, Oberkochen, Germany) was conducted on one slice in each group to observe the morphology of *E. faecalis* biofilm on the dentin. Furthermore, the treated dentin slices were stained with LIVE/DEAD BacLight fluorescence dye (Invitrogen Molecular Probes, Eugene, OR, USA) containing SYTO 9 and PI for 30 min according to the manufacturer's instructions, and then rinsed with PBS. Subsequently, three randomly selected areas of each dentin slice were scanned using a confocal laser scanning microscope (CLSM, TCS SP8, Leica, Wetzlar, Germany). CLSM images were reconstructed into a three-dimensional model and analyzed with Leica confocal software LAS X (Leica Microsystems). The percentage of red fluorescence in all scan slices indicated the proportion of dead bacteria in each group. Each group included three dentin slices.

### Microhardness of Dentin

Dentin slices with dimensions of  $4 \times 4 \times 1$  mm were prepared from the extracted wisdom teeth, and all dentin slices were cleaned as described above. Three original dentin slices from each group were examined using a micro-Vickers hardness tester (HXD-100TMC/LCD, Shanghai Taiming Optical Instrument Co., Ltd. Ltd., Shanghai, China) under a load of 0.4903 N for 10 s, and the average microhardness was calculated at six random points on each dentin slice. Then dentin slices were incubated with PBS, Au@AgNPs, Au@AgNPs+NIR, 2% CHX, or 2.5% NaClO for 10 min, respectively. Subsequently, dentin slices were washed with ddH<sub>2</sub>O to remove any remnant medicine, and microhardness was measured again. After that, the microhardness of untreated and treated dentin slices was compared and analyzed.



## Antibacterial Mechanisms of Au@AgNPs with PTT Against *E. faecalis*

### Bacterial Morphology Observation

Morphological changes in *E. faecalis* were observed using field-emission scanning electron microscopy (FE-SEM, Clara, Tescan, Brno, Czech Republic). *E. faecalis* suspension ( $5 \times 10^6$  CFUs/mL) was incubated with Au@AgNPs (150  $\mu\text{g/mL}$ ) for 10 min with or without irradiation with an 808 nm laser. The bacterial suspension in PBS was used as a blank control. The bacterial suspensions were washed by centrifugation at 3000 rpm at 4°C. The resuspended bacteria in 30  $\mu\text{L}$  of PBS were gently placed on glass coverslips and air-dried. Subsequently, they were quickly fixed, dehydrated, and treated with HMDS (Sinopharm Chemical Reagent Co. Ltd., Shanghai, China). The samples were dried and sputter-coated with gold before scanning using FE-SEM.

Furthermore, cytoarchitectural changes in *E. faecalis* ( $10^9$  CFUs/mL) incubated with Au@AgNPs (300  $\mu\text{g/mL}$ ), with or without NIR irradiation, were analyzed by TEM (HT7800, HITACHI, Tokyo, Japan). After 10 min of incubation, the Au@AgNPs-treated bacteria were collected by centrifugation at 3000 rpm for 5 min. The bacteria were then prepared by fixation, dehydration, infiltration embedding, oven-curing, slicing using an ultramicrotome (LEICA UC7, Leica, Wetzlar, Germany), and staining before TEM observation. In addition, the free-stained samples were subjected to elemental distribution mapping by TEM.

### Measurement of Nucleic Acid Leakage

When the cell membrane is disrupted, the cytoplasmic contents are released into the culture medium. In brief, *E. faecalis* suspension ( $10^9$  CFUs/mL) was incubated with Au@AgNPs (300  $\mu\text{g/mL}$ ) for 10 min with or without NIR irradiation, immediately centrifuged at 12,000 rpm for 5 min, and the supernatant liquid was collected in the DNase-/RNase-free microcentrifuge tube. An untreated *E. faecalis* suspension was used as a blank control, and Au@AgNPs without bacterial suspension was used as background control. The final calculated OD value of *E. faecalis* in the NPs groups was the OD value minus the background value to exclude NPs intervention. Each group was tested three times, and the mean value of the three measurements was used for statistical analysis. The OD was recorded using a NanoDrop 2000 UV-vis Spectrophotometer (Thermo Scientific, Massachusetts, Waltham, USA) at 260 nm.

### Adenosine Triphosphate (ATP) Assay

ATP levels were measured using an Enhanced ATP assay kit (Beyotime Biotechnology, Shanghai, China). In brief, the bacterial suspension ( $10^9$  CFUs/mL) was incubated with Au@AgNPs (200  $\mu\text{g/mL}$ ) with or without irradiation with an 808 nm laser for 10 min, and an untreated *E. faecalis* suspension was used as a blank control. The bacteria were lysed and the supernatant was collected by centrifugation, and the lysed samples were placed on ice to avoid ATP degradation. The luminescence was measured using a fluorescence microplate reader. ATP concentrations were determined by comparison with the ATP standard curves. In addition, the protein concentration of the supernatant was determined using bicinchoninic acid assay (BCA, Biosharp, Hefei, China). Finally, the ATP concentration was recorded as nmol/mg. Each group was tested three times, and the mean value of the three measurements was used for statistical analysis.

### Reactive Oxygen Species (ROS) Detection

*E. faecalis* suspension ( $10^9$  CFUs/mL) was incubated with DCFH-DA (10  $\mu\text{M}$ ) (Beyotime Biotechnology, Shanghai, China) at 37°C for 30 min and mixed upside down every 4 min. The *E. faecalis* suspension was then centrifuged and washed with PBS. Subsequently, *E. faecalis* suspension was incubated with Au@AgNPs (150  $\mu\text{g/mL}$ ) with or without irradiation with an 808 nm laser for 2 min, and the untreated *E. faecalis* suspension was used as a blank control. After incubation for 30 min, bacterial suspensions were centrifuged and resuspended in PBS. For quantitative analysis, 100  $\mu\text{L}$  of bacterial suspension from each group was transferred into a 96-well microplate to examine the fluorescence intensities at excitation and emission wavelengths of 488 and 525 nm, respectively, using a fluorescence microplate (Synergy H1, BioTek, Vermont, USA). Each group was tested three times, and the mean value of the three measurements was used for statistical analysis.

## Detection of Hydroxyl Radical

One milliliter of *E. faecalis* suspension ( $10^9$  CFUs/mL) was incubated with Au@AgNPs (200  $\mu\text{g/mL}$ ) with or without irradiation with an 808 nm laser for 10 min, followed by incubation for more than 40 min. After incubation, 50  $\mu\text{L}$  of DMPO was added to the suspensions and the mixture was transferred to a quartz capillary tube for examination using an EPR instrument (EPR, BrukerA200, Germany).

## In vitro Gene Expression Assay

*E. faecalis* suspension ( $10^9$  CFUs/mL) was incubated with Au@AgNPs (200  $\mu\text{g/mL}$ ) with or without irradiation with an 808 nm laser for 10 min, and the untreated *E. faecalis* suspension was used as a blank control. After incubation for 30 min, total RNA from *E. faecalis* was extracted with TRIzol reagent and chloroform, and cDNA was prepared using ABScript III RT Master Mix for qPCR with gDNA Remover (ABclonal Technology Co., Ltd., Wuhan, China). Real-time quantitative PCR (RT-qPCR) was performed to detect relative mRNA expression levels using SYBR Green qPCR Master Mix (Servicebio Technology Co., Ltd., Wuhan, China) on QuantStudio 6 Flex (Applied Biosystems, Waltham, MA, USA). Raw threshold cycle (Ct) values were calculated for relative expression using the  $2^{-\Delta\Delta\text{Ct}}$ . To normalize the expression levels of the 16S was selected as housekeeping gene. The primers used in this study are listed in [Table S1](#) (See [Additional File](#)).

## Cytotoxicity of Au@AgNPs

The cytotoxicity of Au@AgNPs on human periodontal ligament cells (hPDLs) in vitro was assessed using a cell counting kit-8 (CCK-8). Cells were seeded into each well of a 96-well plate ( $5 \times 10^4$  cells/well) and cultured in  $\alpha$ -modified Eagle's medium ( $\alpha$ -MEM) (Gibco Life Technologies, Carlsbad, CA, USA) consisting of 10% of Fetal Bovine Serum (FBS) and 1% penicillin/streptomycin at 37 °C with 5% CO<sub>2</sub> for 24 h. Six repeated wells were included in each group. After 24 h incubation, 100  $\mu\text{L}$   $\alpha$ -MEM and 10  $\mu\text{L}$  different concentrations of Au@AgNPs (50  $\mu\text{g/mL}$ , 100  $\mu\text{g/mL}$ , 200  $\mu\text{g/mL}$ , 400  $\mu\text{g/mL}$ , 600  $\mu\text{g/mL}$ ), 2% CHX, 2.5% NaClO, and PBS were cultured for another 24 h. The medium was then removed and the cells were washed with PBS. Fresh culture medium (100  $\mu\text{L}$ ) and 10  $\mu\text{L}$  CCK-8 (Biosharp, Hefei, China) were added and incubated in the dark for 4 h. The untreated group was used as a blank control, and the wells containing CCK-8 and  $\alpha$ -MEM were used as background controls. One hundred microliters of supernatant from each well were transferred to a new 96-well plate, and the absorbance at 450 nm was measured using a microplate reader (Synergy H1, BioTek, Vermont, USA).

## Statistical Analysis

The sample size for each experiment of this study was mainly determined based on our pilot studies and relevant published literatures. The distribution of data in this study was analyzed using the Shapiro–Wilk test. Data with normal distribution were analyzed using Student's *t*-test or one-way ANOVA with a post hoc Dunnett *t*-test or post hoc Tukey's test, and data violating the normal distribution were analyzed using the non-parametric Mann Whitney test or Kruskal–Wallis analysis of variance with a post hoc Dunn test. The results of the microhardness tests were statistically analyzed using a paired *t*-test. All statistical analyses were performed using GraphPad Prism 9 (San Diego, CA, USA), and the significance level was set at  $p < 0.05$ . For data in normal distribution, mean  $\pm$  standard deviation (SD) was used, and for data violating the normal distribution, median  $\pm$  quartile (ie P25–P75) was used.

## Results

### Characterization of Au@Ag Core-Shell NPs

Schematic illustration of the synthetic process and application of Au@Ag core-shell NPs was shown in [Figure 1A](#). TEM images showed that the Au@AgNPs were monodispersed with a distinct core-shell structure ([Figure 1B](#)). When dispersed in PBS, the Au@AgNPs aggregated ([Figure 1C](#)). Au@AgNPs with various diameters (26, 30, and 35 nm) were synthesized, their size distributions were measured and Energy Dispersive Spectroscopy (EDS) mapping and line scanning showed the existence of the Au core and distribution of the Ag shell of the Au@AgNPs ([Figures 1D–H](#) and [S1–S2](#)). The corresponding Au@AgNPs were named Au@Ag-26, Au@Ag-30, and Au@Ag-35. The XRD patterns further confirmed the synthesis of the Au@AgNPs ([Figure 1I](#)).

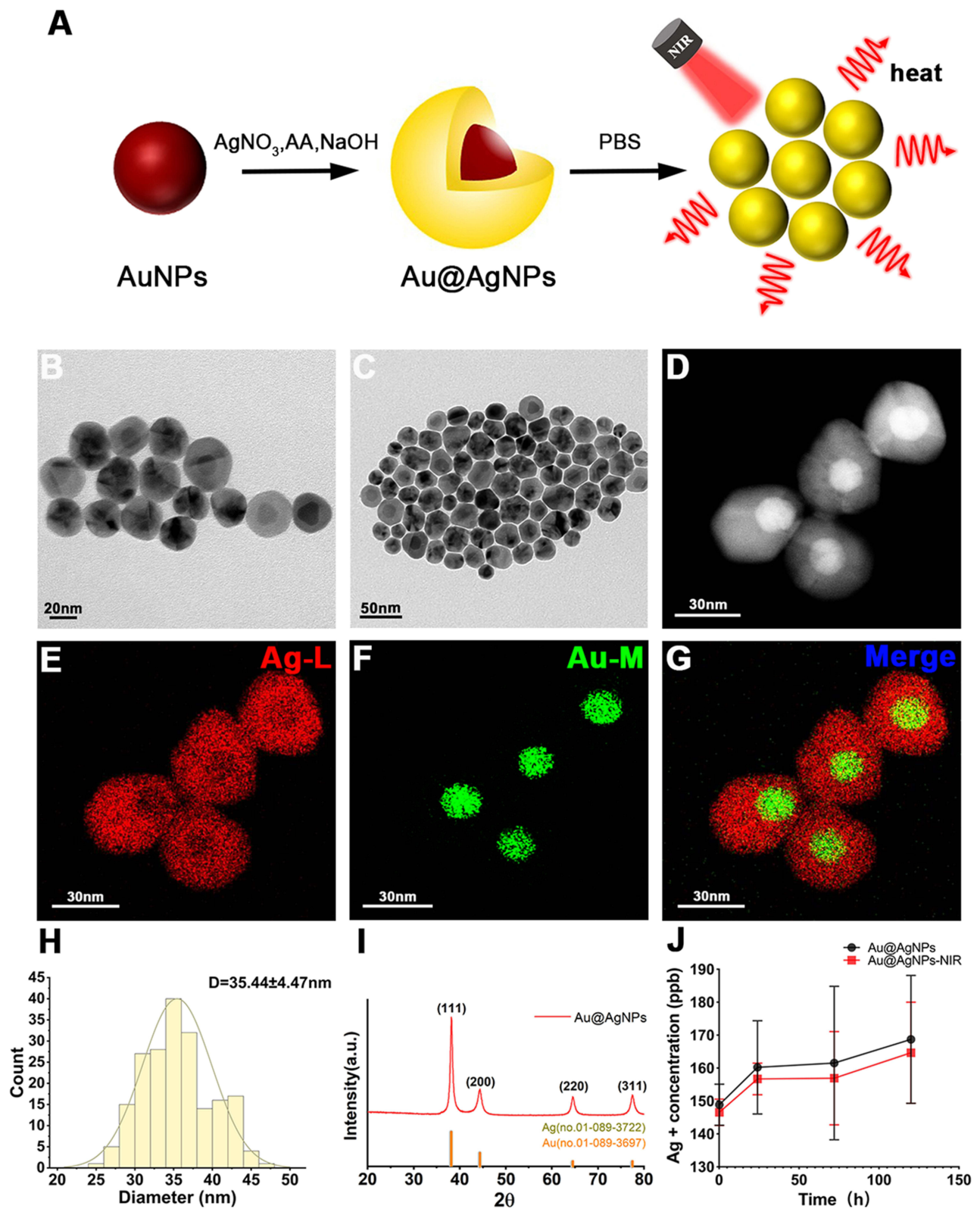


**Figure 1** The characteristics of Au@Ag core-shell NPs. **(A)** Schematic illustration of the synthetic process and application of Au@Ag core-shell NPs. **(B and C)** TEM images of Au@AgNPs-35 incubated in deionized water and PBS. **(D-G)** EDS elemental mapping of Au@AgNPs-35. **(H)** Size distribution of Au@AgNPs-35 in TEM images. **(I)** XRD pattern of Au@AgNPs-35. **(J)** Release profile of Ag<sup>+</sup> from Au@AgNPs-35 with and without NIR.

ICP-MS (Figure 1J) revealed that the amount of  $\text{Ag}^+$  released from Au@AgNPs with or without irradiation by an 808 nm laser in PBS gradually increased over time. There was no significant difference in the amount of released  $\text{Ag}^+$  between the Au@AgNPs with (164.7±15.39 ppb) and without (168.7±19.42 ppb) the 808 nm laser ( $p>0.05$ ).

With the addition of PVP and  $\text{AgNO}_3$ , the hydrodynamic size of the NPs gradually increased, and the zeta potential of the NPs first increased and then decreased (Figure 2A and B). The UV-Vis spectra of AuNPs showed an absorbance peak at approximately 520 nm, and Au@AgNPs with different Ag shell thicknesses showed an absorbance peak at approximately 410 nm. When Au@AgNPs were dispersed in PBS, the plasma absorption near the NIR region was enhanced by increasing the size of the Au@AgNPs (Figure 2C and D).

In terms of the photothermal effect, Au@AgNPs displayed a shell size-dependent temperature profile after exposure to the 808 nm laser (Figures 2E and S3). In addition, temperature elevation was positively correlated with material concentrations (Figures 2E and S3) or laser powers (Figure 2F). Favorable photothermal stability was observed in Au@Ag-35 NPs with repeated irradiation by an 808 nm laser (Figure 2G). Therefore, Au@Ag-35 NPs was selected for the subsequent experiments. As shown in represent thermal images with different concentrations of Au@Ag-35 NPs in root canals (Figure 2H-K), the higher was the concentration of Au@Ag-35 NPs, the higher would the temperature increase. Notably, the temperature of the cementum was lower than that of the dentin. In addition, the temperature decreased from the cervical to the apical parts of the tooth.

## Antimicrobial Effects Against Planktonic Original and $\text{Ag}^+$ -Resistant *E. faecalis*

### Antimicrobial Effects Against Original *E. faecalis*

The antibacterial effect against Au@AgNPs with and without 808 nm laser irradiation for 10 min is shown in Figure 3A-Q. In the NPs group without 808 nm laser irradiation, there was no significant inhibitory effect with increasing Au@AgNPs concentrations ( $p>0.05$ ). When the concentration of Au@AgNPs was not less than 100  $\mu\text{g}/\text{mL}$  in the NPs group with 808 nm laser irradiation, the bacterial viability (71.33%±33.71%) was significantly reduced compared with the blank control

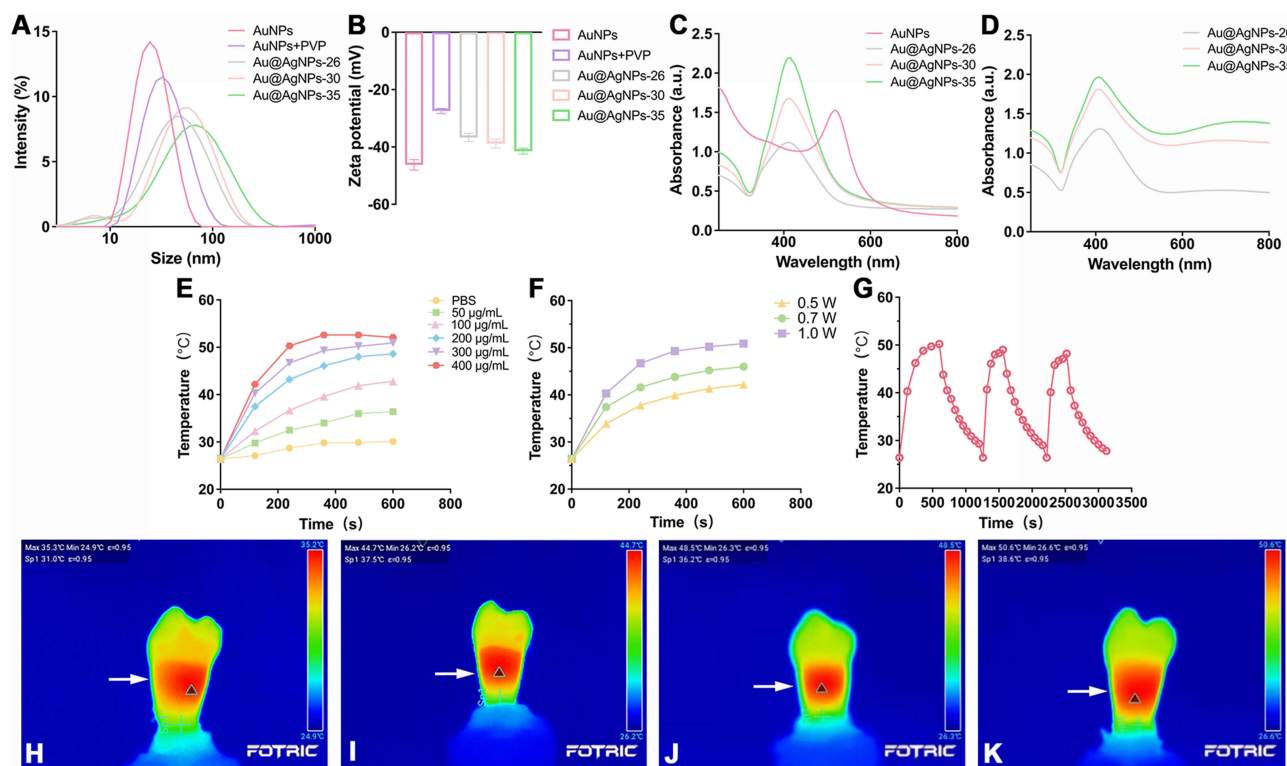


**Figure 2** The characteristics and photothermal correlational properties of Au@AgNPs. (A and B) Dynamic light scattering and Zeta potential of products in the formation process of Au@AgNPs and different shell thickness Au@AgNPs. (C and D) UV-vis-NIR spectra of Au@AgNPs incubated in deionized water and PBS (E) PT curves of Au@AgNPs-35 with different concentrations. (F) PT curves of Au@AgNPs-35 under irradiation of different laser powers. (G) PT cycle tests of Au@AgNPs-35 under laser irradiation. (H-K) Thermal images of Au@AgNPs-35 with 100  $\mu\text{g}/\text{mL}$ , 200  $\mu\text{g}/\text{mL}$ , 300  $\mu\text{g}/\text{mL}$ , 400  $\mu\text{g}/\text{mL}$  respectively (The white arrow pointing to cementum).



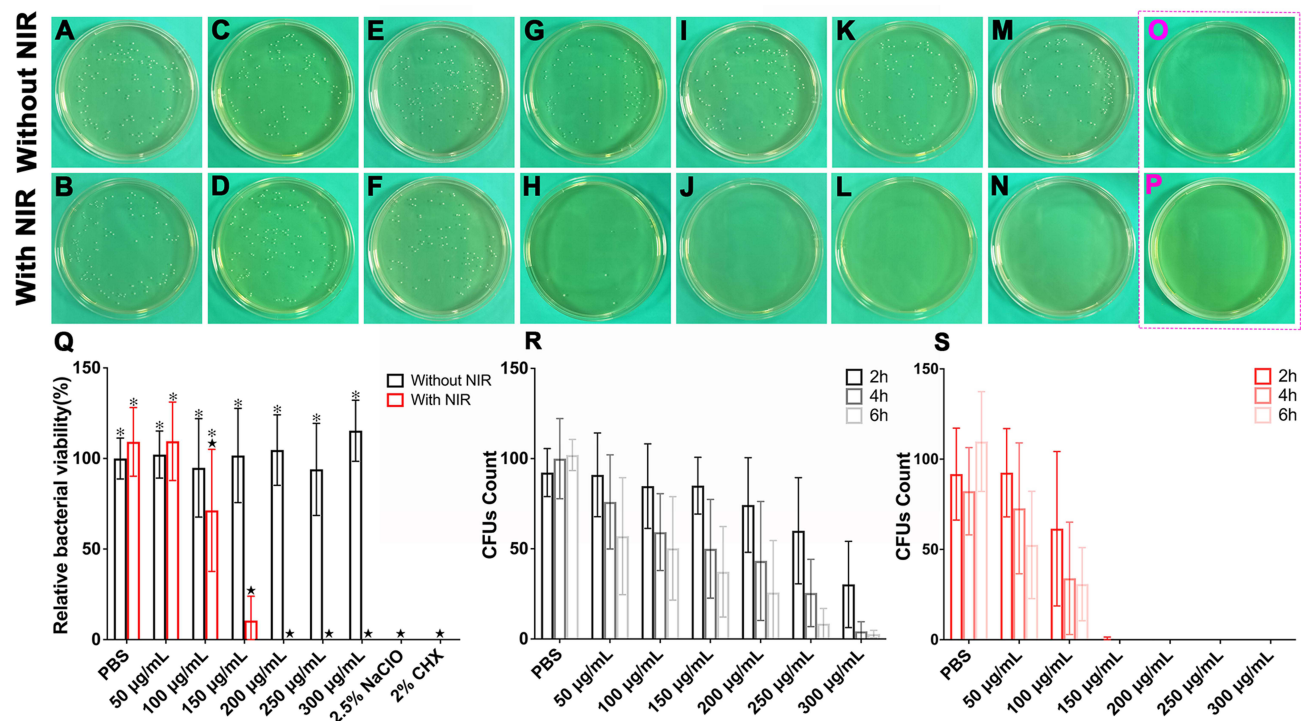


**Figure 3** Antibacterial activities assessment of Au@AgNPs with and without PTT against *E. faecalis* in vitro. Representative images of bacteria colonies grown on BHI agar. (A and B) blank control group (PBS). (C and D) Au@AgNPs-35 (50 µg/mL). (E and F) Au@AgNPs-35 (100 µg/mL). (G and H) Au@AgNPs-35 (150 µg/mL). (I and J) Au@AgNPs-35 (200 µg/mL). (K and L) Au@AgNPs-35 (250 µg/mL). (M and N) Au@AgNPs-35 (300 µg/mL). (O) 2% CHX. (P) 2.5% NaClO. (Q) Comparison of bacterial viability among NPs groups with and without NIR for 10 min. (R) Comparison of bacterial CFUs among NPs groups without NIR at different time points. (S) Comparison of bacterial CFUs among NPs groups with NIR at different time points. (The black star indicated significant difference when compared with blank control (PBS), The black asterisk indicated significant difference when compared with 2% CHX or 2.5% NaClO,  $p < 0.05$ ).

( $p < 0.05$ ). When compared to 2.5% NaClO or 2% CHX, Au@AgNPs at the concentration of no less than 150 µg/mL had similar antibacterial effects (10.50%±13.49%) in NPs group with NIR irradiation ( $p > 0.05$ ). (Figure 3Q).

In addition, Au@AgNPs showed sustained antibacterial properties regardless of the presence or absence of 808 nm laser irradiation. A declining tendency was observed in CFUs with prolonged exposure times and increased concentrations (Figure 3R and S).

### Establishment and Antimicrobial Effects Against Ag<sup>+</sup>-Resistant *E. faecalis*

The MIC for *E. faecalis* was 128 µg/mL. After the induction of Ag<sup>+</sup>-resistant *E. faecalis*, the value of OD 600 nm the Ag<sup>+</sup>-resistant *E. faecalis* suspension ( $10^8$  CFUs/mL in 2MIC AgNO<sub>3</sub> and  $10^7$  CFUs/mL in 1MIC and 2MIC AgNO<sub>3</sub>) significantly increased ( $p < 0.001$ ) (Figure 4A). When the concentration of Au@AgNPs was not less than 200 µg/mL in the NPs group with NIR irradiation, the bacterial viability [17.50% (0–35%)] was significantly reduced compared with the blank control ( $p < 0.05$ ) (Figure 4B).

When Ag<sup>+</sup>-resistant *E. faecalis* was exposed to AgNO<sub>3</sub> for 10 min, no significant difference was observed between the blank control and AgNO<sub>3</sub>-treated groups ( $p > 0.05$ ). However, the CFUs of Ag<sup>+</sup>-resistant *E. faecalis* treated with Au@AgNPs with PTT were significantly lower than those of the blank control ( $p < 0.01$ ) (Figure 4C).

### Antibiofilm Effects Against *E. faecalis* Biofilm on Dentin

The SEM images (Figure 5) confirmed that the morphology of Au@AgNPs-treated bacteria under NIR irradiation showed different degrees of cell perforation and breakdown (Figure 5C-H) compared with blank control (Figure 5A and B). Besides, there were still some intact bacteria on dentin slices in 2% CHX-treated group (Figure 5I and J), but no residual bacteria were found on dentin slices in 2.5% NaClO-treated group (Figure 5K and L). As shown in Figure 6, Au@AgNPs with PTT and 2% CHX showed significant antibiofilm activity ( $p < 0.05$ ). Au@AgNPs with PTT displayed a concentration-dependent



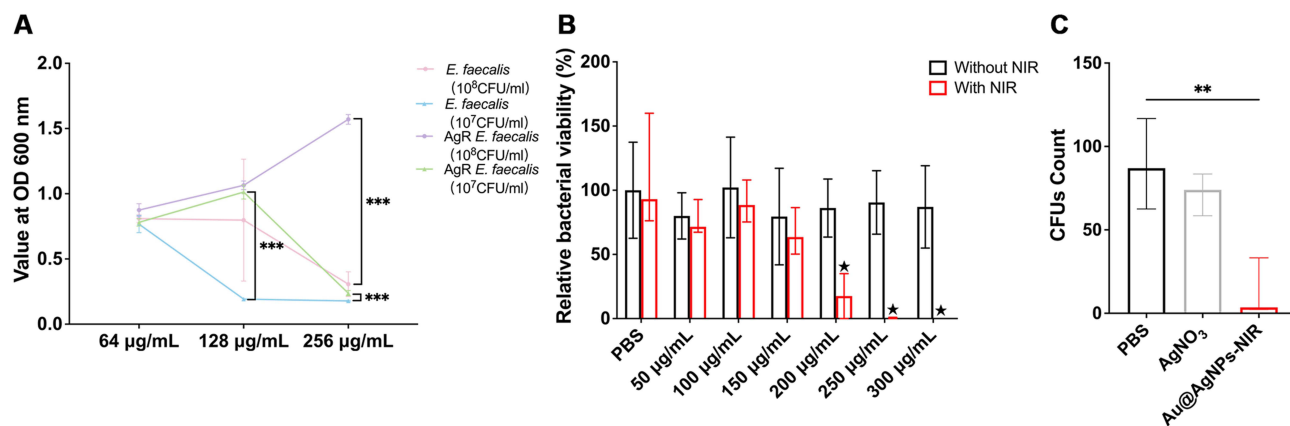


**Figure 4** Establishment and antimicrobial effects against Ag<sup>+</sup>-resistant *E. faecalis*. **(A)** Comparison of value at OD600 nm between *E. faecalis* and Ag<sup>+</sup>-resistant *E. faecalis*. **(B)** Comparison of bacterial viability among NPs groups with and without NIR for 10 min. **(C)** Comparison of bacterial CFUs between AgNO<sub>3</sub> and Au@AgNPs-NIR treated groups. (The black star indicated significant difference when compared with blank control (PBS), \**p* < 0.05; \*\**p* < 0.01; \*\*\**p* < 0.001).

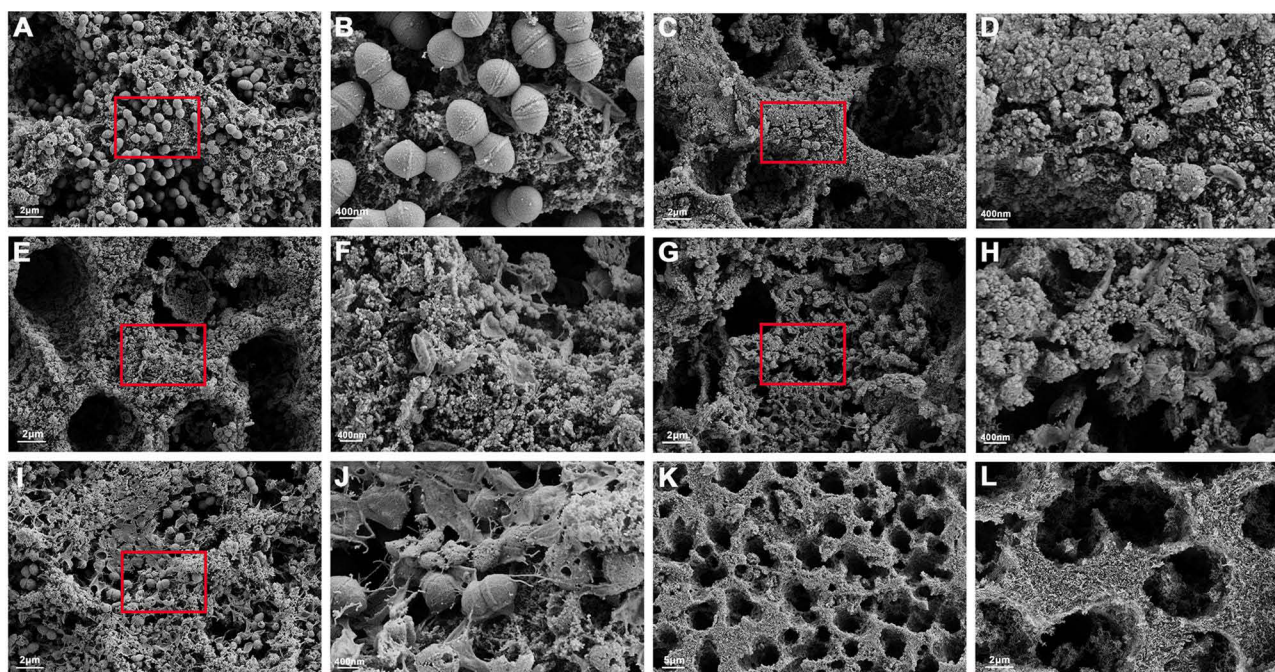


**Figure 5** Antibiofilm assessment of Au@AgNPs PTT by SEM. **(A and B)** *E. faecalis* biofilm treated with PBS. (A×5000, B×20000) **(C and D)** *E. faecalis* biofilm treated with Au@AgNPs-35 (400 µg/mL) PTT. (C×5000, D×20000) **(E and F)** *E. faecalis* biofilm treated with Au@AgNPs-35 (500 µg/mL) PTT. (E×5000, F×20000) **(G and H)** *E. faecalis* biofilm treated with Au@AgNPs-35 (600 µg/mL) PTT. (G×5000, H×20000) **(I and J)** *E. faecalis* biofilm treated with 2% CHX. (I×5000, J×20000) **(K and L)** *E. faecalis* biofilm treated with 2.5% NaClO. (K×1600, L×5000) (The red rectangle refers to the zoomed-in areas).

antibiofilm activity. No significant difference was observed in the percentage of red fluorescence among 2% CHX (65.11% ± 7.51%), 400 µg/mL (67.33% ± 7.81%), and 500 µg/mL (73.56% ± 5.86%) of Au@AgNPs with PTT (*p* > 0.05). There was no significant difference in PTT between 500 µg/mL and 600 µg/mL (80.44% ± 5.48%) of Au@AgNPs (*p* > 0.05). Whereas 600 µg/mL of Au@AgNPs with PTT was significantly more effective than 2% CHX at killing bacteria in biofilms (*p* < 0.05).

## Effect on Microhardness of Dentin

As shown in [Figure S4A](#), there was no significant difference in the changes in dentin microhardness between the groups before and after incubation (*p* > 0.05), except in the 2.5% NaClO group. The 2.5% NaClO group displayed obvious reduction in the dentin microhardness (*p* < 0.05).

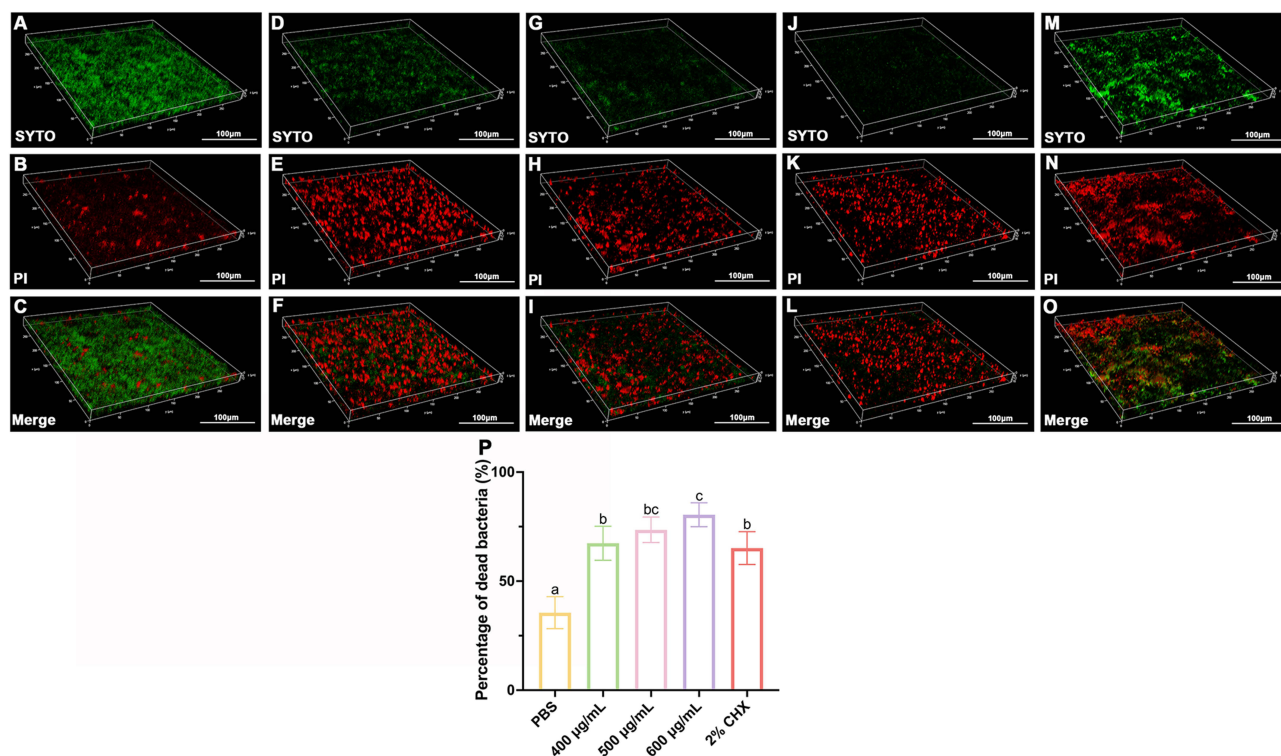


**Figure 6** Antibiofilm assessment of Au@AgNPs PTT by CLSM. (A-C) *E. faecalis* biofilm treated with PBS. (D-F) *E. faecalis* biofilm treated with Au@AgNPs-35 (400 µg/mL) PTT. (G-I) *E. faecalis* biofilm treated with Au@AgNPs-35 (500 µg/mL) PTT. (J-L) *E. faecalis* biofilm treated with Au@AgNPs-35 (600 µg/mL) PTT. (M-O) *E. faecalis* biofilm treated with 2% CHX. (P) Comparison of percentage of dead bacteria among groups. (Green: live bacteria; Red: dead bacteria. Different lowercase letters represent statistical differences among groups,  $p < 0.05$ ).

## Antibacterial Mechanisms of Au@AgNPs with PTT Against *E. faecalis*

### Destruction of Bacterial Wall and Membrane Integrity

SEM and TEM were used to observe the bacterial morphology and structural changes following treatment. Untreated *E. faecalis* cells had a smooth cell wall (Figure 7A). Even after irradiation with an 808 nm laser for 10 min, the morphology and cell wall of the bacteria did not change significantly (Figure 7B). When treated with Au@AgNP regardless of the presence or absence of 808 nm laser irradiation, the bacterial cells shrank and wrinkled, and morphological damage was more severe after laser irradiation (Figure 7C and D).

The structural change in *E. faecalis* treated with Au@AgNPs with or without 808 nm laser irradiation was verified by TEM (Figure 7E-L). Most Au@AgNPs-treated bacteria showed cell membrane lysis, intracellular voids, and disintegration of intracellular structures after 10 min of laser-induced treatment. Only a few Au@AgNP-treated bacteria exhibited slight shrinkage and aggregation of the cytoplasm when no laser treatment was applied. The distribution of Au@AgNPs among the bacteria was determined using TEM (Figure 7M-T). Most Au@AgNPs were scattered among the bacteria, and some Au@AgNPs adhered to the cell wall of *E. faecalis*.

The amount of RNA released from Au@AgNP-treated bacteria after laser irradiation was remarkably higher than in the other groups ( $p < 0.05$ ) (Figure 8A).

### ATP Assay

A significant reduction in ATP levels was observed in Au@AgNPs-treated *E. faecalis* after NIR irradiation ( $p < 0.01$ ). No significant difference was observed in the amount of ATP produced by *E. faecalis* with laser irradiation or Au@AgNPs alone compared to the blank control ( $p > 0.05$ ) (Figure 8B).



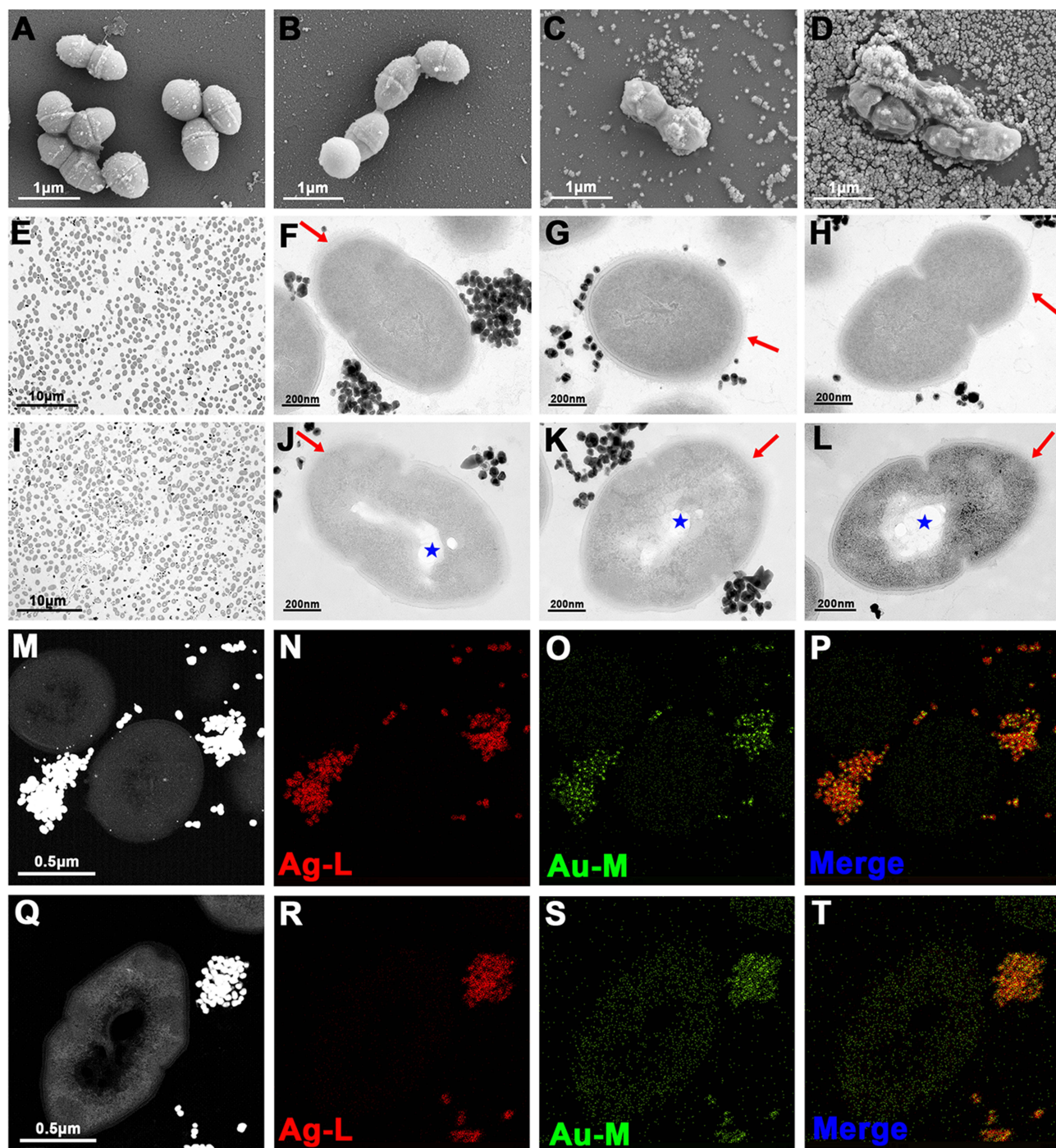


**Figure 7** Morphology and structure deformation of *E. faecalis* incubated with Au@AgNPs at the presence or absence of NIR irradiation. (A) SEM images of *E. faecalis* treated by PBS without NIR. (B) SEM images of *E. faecalis* treated by PBS with NIR. (C) SEM images of *E. faecalis* treated by Au@AgNPs-35 without NIR. (D) SEM images of *E. faecalis* treated by Au@AgNPs-35 with NIR. (E-H) TEM images of *E. faecalis* incubated with Au@AgNPs-35. (I-L) TEM images of *E. faecalis* treated by Au@AgNPs-35 with NIR. (M-P) Elemental mapping of *E. faecalis* incubated with Au@AgNPs-35. (Q-T) Elemental mapping of *E. faecalis* treated by Au@AgNPs-35 with NIR. (The blue star indicated intracellular voids and the disintegration of intracellular structures; The red arrows indicated the cell membrane defect.)

### Reactive Oxygen Species (ROS) Detection

Regardless of the presence or absence of NIR irradiation, Au@AgNPs groups led to higher levels of ROS in *E. faecalis* compared to the non-treated groups ( $p < 0.01$ ), and there was no significant difference between the NPs groups ( $p > 0.05$ ) (Figure 8C). A DMPO spin-trapping system was used to detect the generation of  $\cdot\text{OH}$  radicals. Only in the presence of Au@AgNPs can  $\cdot\text{OH}$  be produced (Figure 8D).

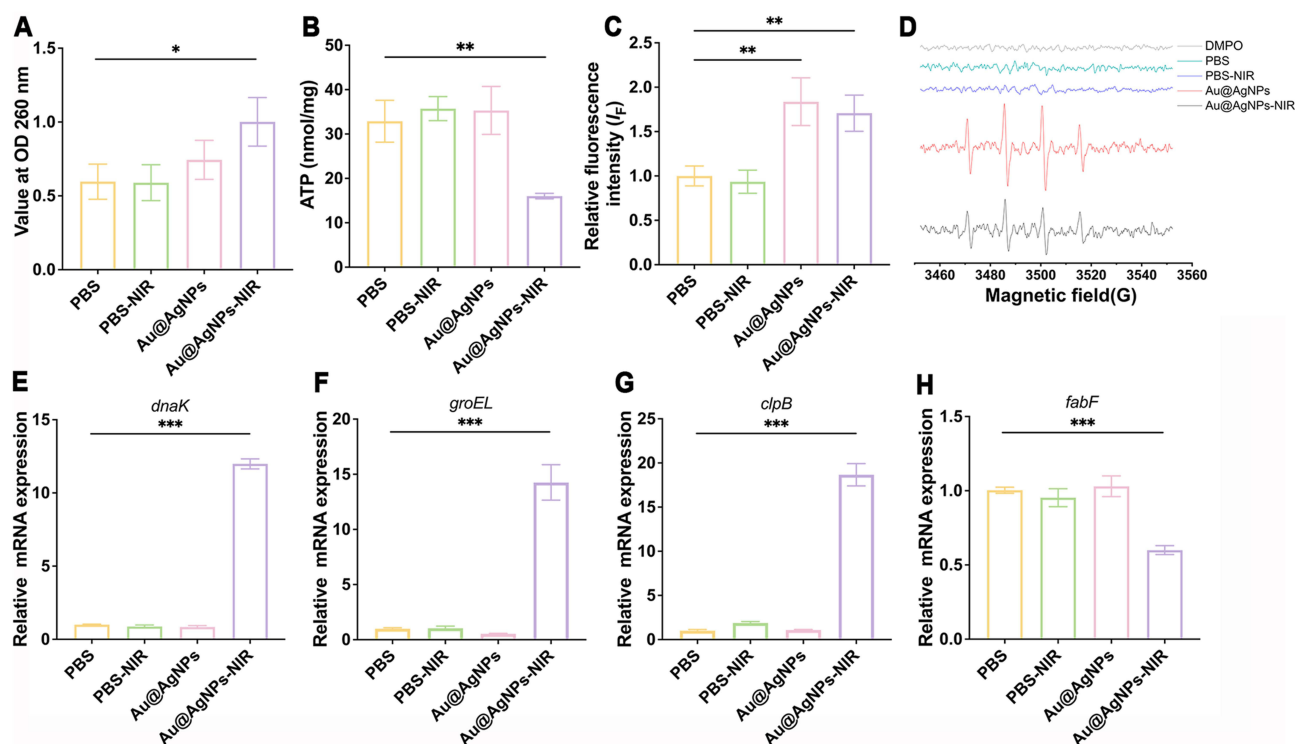


**Figure 8** Potential antimicrobial mechanisms of Au@AgNPs with PTT. (A) RNA concentration released from *E. faecalis* after exposure to Au@AgNPs-35 with or without NIR. (B) ATP assay of *E. faecalis* after exposure to Au@AgNPs-35 with or without NIR. (C) DCFH-DA test of *E. faecalis* after exposure to Au@AgNPs-35 with or without NIR. (D) EPR spectra of *E. faecalis* after exposure to Au@AgNPs-35 with or without NIR. (E-H) Relative mRNA expression of *dnaK*, *groEL*, *clpB* and *fabF* in *E. faecalis* after exposure to Au@AgNPs-35 with or without NIR. (\* $p < 0.05$ ; \*\* $p < 0.01$ ; \*\*\* $p < 0.001$ ).

### Related Gene Expressions

The expression of the heat-shock genes *dnaK*, *groEL*, and *clpB* and the temperature-sensitive enzyme gene *fabF* are shown in Figure 8E-H. The results showed that upregulation of *dnaK*, *groEL*, and *clpB* was induced by Au@AgNPs with NIR irradiation compared with the blank control ( $p < 0.001$ ). However, expression of *fabF* was significantly suppressed after treated by Au@AgNPs with NIR irradiation ( $p < 0.001$ ).

### Cytotoxicity

The results of CCK-8 test on the human periodontal ligament cells (hPDLs) indicated that all nanoparticles groups had no suppressive effect on the proliferation of hPDLs compared with the blank control ( $p > 0.05$ ), but 2.5% NaClO or 2% CHX both significantly inhibited cell growth ( $p < 0.05$ ) (Figure S4B).

### Discussion

Bimetallic gold-silver nanoparticles have a wide range of applications in biomedical field due to its broad-spectrum antibacterial capabilities.<sup>15</sup> In this study, different shell thickness of Au@Ag core-shell NPs were successfully synthesized by controllable reduction of AgNO<sub>3</sub> onto the Au seeds based on seeded growth strategy,<sup>27</sup> which was confirmed by TEM, XRD and EDS. In addition, the DLS and Zeta measurements demonstrated stability. The surface plasmon resonance absorption peak of monodispersed Au@Ag core-shell NPs is not in the near-infrared region, which weakens photothermal conversion. PBS is commonly used as a physiological buffer to maintain the biological activity of the cells. This study found that PBS can induce the aggregation of Au@Ag core-shell NPs to enhance their resonance in the NIR region, and the thicker the shell, the higher the photothermal conversion efficiency.

Meanwhile, photothermal therapy enhanced the antibacterial ability of the Au@Ag core-shell NPs. The time-dependent antibacterial ability can be explained by the continuous release of Ag<sup>+</sup> from Au@AgNPs. This is consistent with previous studies on the antibacterial effects after 24 hours.<sup>14</sup> In terms of antibiofilm test, Au@AgNPs combined with PTT was superior to 2%

CHX. However, the biofilm removing effect of Au@AgNPs combined with PTT was inferior to 2.5% NaClO because of its inability to dissolve organic matrix inside the biofilm, but there was no adverse effect on dentin strength compared with 2.5% NaClO. In addition, compared with 2% CHX or 2.5% NaClO, Au@AgNPs showed lower cytotoxicity.

The release of cytoplasmic constituents from bacteria with compromised cell membranes implies that bacterial death is directly associated with the destruction of the bacterial membrane.<sup>28,29</sup> As shown in this study, the addition of PTT can cause cell membrane disruption and loss of intracellular content in *E. faecalis* treated with Au@AgNPs in a short period of time. However, fewer Au@AgNPs were found attached to the bacteria, probably because of the formation of aggregates and the incubation time. It was envisioned that the release of Ag<sup>+</sup> from Au@AgNPs aggregates with PTT would affect the antibacterial efficiency in a short period. Oxidative stress is considered a bactericidal mechanism of Ag<sup>+</sup>.<sup>15,30</sup> The elevated levels of intracellular ROS and ·OH in *E. faecalis* incubated with Au@AgNPs demonstrated oxidative stress in bacterial cells. Various gold-silver nanostructures have also been reported to exert antibacterial effects through the production of ROS.<sup>29,31</sup> Although a previous study reported that released Ag<sup>+</sup> from AgNPs disrupted ATP production, short-term exposure to Au@AgNPs alone did not inhibit ATP production in this study.<sup>32</sup>

Heat-shock proteins (HSPs) are a small set of proteins that organisms synthesize in response to sudden temperature increases.<sup>33</sup> HSPs such as HSP70/DnaK and HSP60/GroEL are induced at high temperature to promote the degradation of denatured proteins to protect cells from stress.<sup>33</sup> *clpB*, a class III heat-shock gene, is involved in thermotolerance and virulence of *E. faecalis*.<sup>34</sup> ClpB had been shown to act synergistically with the DnaK system to remodel or dissolve protein aggregates that arise after heat stress in *E. coli*.<sup>35,36</sup> The collaboration between ClpB and DnaK system required ATP hydrolyzation.<sup>35</sup> It could be inferred that the decline in ATP generation in Au@AgNPs with PTT treated group was related to heat stress. To our knowledge, *E. faecalis* can grow at temperatures ranging from 5 to 50 °C,<sup>37</sup> even survive for 30 min at 60 °C.<sup>38</sup> In the present study, heat shock responses, especially the upregulated expression of *dnaK*, *groEL* and *clpB*, may also involve in the mechanism of *E. faecalis* coping with the heat stress of Au@AgNPs with PTT. Based on the above information, it can be confirmed that Ag<sup>+</sup> released from Au@AgNPs compromised the heat adaptation of *E. faecalis*. *E. faecalis* can also modify the composition of phospholipid acyl chains in response to changes in the environmental temperature, which is mediated by FabF. Inactivation of FabF at high temperatures resulted in the reduction of cell membrane fluidity.<sup>39</sup> It could be speculated the reduced membrane fluidity and decreased ATP production, which might decrease the efflux of silver ions, thus enhancing Ag<sup>+</sup> sensitivity. Moreover, bacterial type II fatty acid synthesis (FASII) is a vital aspect of bacterial physiology, not only for the formation of membrane but also to produce intermediates of vitamin production.<sup>40</sup> FabF was reported to be one of the enzyme targets in FASII,<sup>40</sup> and the expression of *fabF* was significantly inhibited by Au@AgNPs with PTT, which might indicate that Au@AgNPs with PTT was a new FASII inhibitor to attenuate bacterial resistance. Au@AgNPs combined with PTT showed a higher sensitivity to Ag<sup>+</sup>-resistant bacteria, indicating that photothermal treatment could enhance the sensitivity of bacteria to Ag<sup>+</sup>. A pattern diagram of the antimicrobial mechanism of Au@AgNPs with PTT is shown in Figure 9.

Previous studies have indicated that high temperature root canal irrigation could be used as an alternative process for the elimination of microorganisms from the root canal system.<sup>41,42</sup> Increasing the temperature could optimize the effectiveness of NaClO in killing *E. faecalis* while minimizing the damage to dentin.<sup>43</sup> In addition, Cao et al also reported that Au@Cu<sub>2-x</sub>NPs with photothermal activity could catalyze H<sub>2</sub>O<sub>2</sub> to effectively degrade *E. faecalis* biofilm in root canals.<sup>27</sup> This study revealed the great potential of Au@AgNPs combined with PTT for root canal disinfection. However, heat generation resulting in potential thermal injury to the periodontium may be a concern. From the representative thermal images in this study, the rising temperature was concentration-dependent, and the highest temperature was located at the cervical area of the roots, which may be attributed to the large volume of the root canal in this part as well as its proximity to the laser. In addition, cementum with poor heat conductivity provides better protection for the periodontal tissue. Cen et al suggested that the cooling capacity of periodontal blood flow cannot be neglected during heat transfer.<sup>44</sup> Despite this, its validity of antimicrobial effects and safety of thermal to periodontal tissue in vivo still need to be further investigated in the future because of the limitations of in vitro experiments. What's more, how to effectively and safely conduct heat to the root tip in the long and narrow root canals also needs further studies.



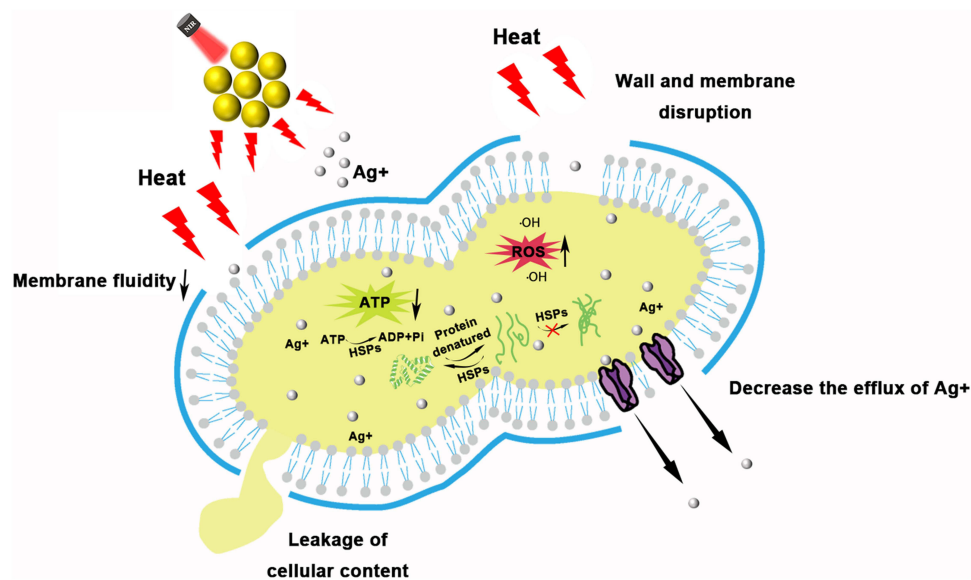


**Figure 9** Illustration of antimicrobial mechanism of Au@AgNPs with PTT.

## Conclusion

In summary, Au@AgNPs with PTT showed enhanced antibacterial activity against *E. faecalis* in either planktonic form or biofilms on dentin in a concentration- and time-dependent manner. The enhanced antibacterial effect was due to the release of Ag<sup>+</sup>, disruption of the bacterial cell walls and membranes, induction of oxidative stress, and inhibition of ATP production. It also showed low cytotoxicity and no adverse effects on the dentin strength. In addition, Au@AgNPs with PTT have an effective bactericidal ability against Ag<sup>+</sup>-resistant *E. faecalis*, which indicates that photothermal treatment can enhance silver sensitivity. These findings might indicate that Au@AgNPs combined with PTT may offer a novel therapeutic strategy for root canal disinfection of teeth, and further studies to investigate the validity and biocompatibility in vivo are needed for potential clinical applications.

## Abbreviations

RAP, refractory apical periodontitis; *E. faecalis*, *Enterococcus faecalis*; PTT, photothermal therapy; AgNPs, silver nanoparticles; MDR, multidrug-resistant; NIR, near-infrared; LSPR, localized surface plasmon resonance; PBS, phosphate-buffered saline; DLS, Dynamic Light Scattering; TEM, transmission electron microscopy; XRD, X-ray diffraction; ICP-MS, inductively coupled plasma mass spectrometry; CFUs, colony-forming units; BHI, brain heart infusion; MIC, minimal inhibitory concentration; OD, optical density; FE-SEM, field emission scanning electron microscopy; CLSM, confocal laser scanning microscopy; ATP, adenosine triphosphate; ROS, reactive oxygen species; OH, hydroxyl radical; hPDLs, human periodontal ligament cells; EDS, Energy Dispersive Spectroscopy; HSPs, Heat-shock proteins.

## Ethics Approval and Consent to Participate

The tooth samples and hPDLs used in this study were collected with the approval of the Ethics Committee of the School and Hospital of Stomatology, Wuhan University [WDKQ2023-B66]. The informed consent was obtained from the study participants prior to study commencement.

## Funding

The authors would like to thank the funding support from the National Natural Science Foundation of China (Grant Nos. 82270968 and 82170943), Top Youth Talent in Medicine Program of Hubei Province, China, and Fundamental Research Funds for the Central Universities, China (2042022kf1165).

## Disclosure

The authors declare no competing interests in this work.

## References

1. Deng Z, Lin B, Liu F, et al. Role of *Enterococcus faecalis* in refractory apical periodontitis: from pathogenicity to host cell response. *J Oral Microbiol.* 2023;15(1):2184924.
2. Stuart CH, Schwartz SA, Beeson TJ, et al. *Enterococcus faecalis*: its role in root canal treatment failure and current concepts in retreatment. *J Endod.* 2006;32(2):93–98.
3. Tennert C, Fuhrmann M, Wittmer A, et al. New bacterial composition in primary and persistent/secondary endodontic infections with respect to clinical and radiographic findings. *J Endod.* 2014;40(5):670–677.
4. Zhang C, Du J, Peng Z. Correlation between *Enterococcus faecalis* and Persistent Intraradicular Infection Compared with Primary Intraradicular Infection: a Systematic Review. *J Endod.* 2015;41(8):1207–1213.
5. Elashiry MM, Bergeron BE, Tay FR. *Enterococcus faecalis* in secondary apical periodontitis: mechanisms of bacterial survival and disease persistence. *Microb Pathog.* 2023;183:106337.
6. García-Solache M, Rice LB. The *Enterococcus*: a Model of Adaptability to Its Environment. *Clin Microbiol Rev.* 2019;32(2):10–128.
7. Chivatxaranukul P, Dashper SG, Messer HH. Dentinal tubule invasion and adherence by *Enterococcus faecalis*. *Int Endod J.* 2008;41(10):873–882.
8. Sánchez-López E, Gomes D, Esteruelas G, et al. Metal-Based Nanoparticles as Antimicrobial Agents: an Overview. *Nanomaterials (Basel).* 2020;10(2).
9. Bolenwar A, Reche A, Dhamdhare N, et al. Applications of Silver Nanoparticles in Dentistry. *Cureus.* 2023;15(8):e44090.
10. Ghahramani Y, Yaghoobi F, Motamedi R, et al. Effect of Endodontic Irrigants and Medicaments Mixed with Silver Nanoparticles against Biofilm Formation of *Enterococcus faecalis*. *Iran Endod J.* 2018;13(4):559–564.
11. Wu D, Fan W, Kishen A, et al. Evaluation of the antibacterial efficacy of silver nanoparticles against *Enterococcus faecalis* biofilm. *J Endod.* 2014;40(2):285–290.
12. Li H, Xu H. Mechanisms of bacterial resistance to environmental silver and antimicrobial strategies for silver: a review. *Environ Res.* 2024;248:118313.
13. Fan W, Sun Q, Li Y, et al. Synergistic mechanism of Ag(+)-Zn(2+) in anti-bacterial activity against *Enterococcus faecalis* and its application against dentin infection. *J Nanobiotechnology.* 2018;16(1):10.
14. Yang LP, Yan WJ, Wang HX, et al. Shell thickness-dependent antibacterial activity and biocompatibility of gold@silver core-shell nanoparticles. *RSC Adv.* 2017;7(19):11355–11361.
15. Singh C, Mehata AK, Priya V, et al. Bimetallic Au-Ag Nanoparticles: advanced Nanotechnology for Tackling Antimicrobial Resistance. *Molecules.* 2022;27(20).
16. Cui J, Sun Q, Duan M, et al. Establishment and characterization of silver-resistant *Enterococcus faecalis*. *Folia Microbiol (Praha).* 2020;65(4):721–733.
17. Salas-Orozco MF, Niño-Martínez N, Martínez-Castañón GA, et al. Proteomic analysis of an *Enterococcus faecalis* mutant generated against the exposure to silver nanoparticles. *J Appl Microbiol.* 2022;132(1):244–255.
18. Aminabad NS, Farshaf M, Akbarzadeh A. Recent Advances of Gold Nanoparticles in Biomedical Applications: state of the Art. *Cell Biochem Biophys.* 2019;77(2):123–137.
19. Ding X, Yuan P, Gao N, et al. Au-Ag core-shell nanoparticles for simultaneous bacterial imaging and synergistic antibacterial activity. *Nanomedicine.* 2017;13(1):297–305.
20. Hussein EA, Zagho MM, Nasrallah GK, et al. Recent advances in functional nanostructures as cancer photothermal therapy. *Int J Nanomed.* 2018;13:2897–2906.
21. Ye X, Shi H, He X, et al. Gold nanorod-seeded synthesis of Au@Ag/Au nanospheres with broad and intense near-infrared absorption for photothermal cancer therapy. *J Mater Chem B.* 2014;2(23):3667–3673.
22. Pan WY, Huang CC, Lin TT, et al. Synergistic antibacterial effects of localized heat and oxidative stress caused by hydroxyl radicals mediated by graphene/iron oxide-based nanocomposites. *Nanomedicine.* 2016;12(2):431–438.
23. Cui J, Duan M, Sun Q, et al. Simvastatin decreases the silver resistance of *E. faecalis* through compromising the entrapping function of extracellular polymeric substances against silver. *World J Microbiol Biotechnol.* 2020;36(4):54.
24. Mohanty A, Fattekar AP, Vernekar AA. All Ag Nanoparticles Are Not the Same: covalent Interactions between Ag Nanoparticles and Nitrile Groups Help Combat Drug- and Ag-Resistant Bacteria. *ChemMedChem.* 2021;16(23):3545–3547.
25. Huang YN, Qian TT, Dang F, et al. Significant contribution of metastable particulate organic matter to natural formation of silver nanoparticles in soils. *Nat Commun.* 2019;10(1):3775.
26. Vuković B, Cvetić Ž, Bendelja K, et al. In vitro study on the immunomodulatory effects of differently functionalized silver nanoparticles on human peripheral blood mononuclear cells. *J Biol Inorg Chem.* 2021;26(7):817–831.
27. Cao J, Sun Q, Shen AG, et al. Nano Au@Cu<sub>2-x</sub>S with near-infrared photothermal and peroxidase catalytic activities redefines efficient antibiofilm-oriented root canal therapy. *Chem Eng J.* 2021;422:12.
28. Liu S, Wei L, Hao L, et al. Sharper and faster “nano darts” kill more bacteria: a study of antibacterial activity of individually dispersed pristine single-walled carbon nanotube. *ACS Nano.* 2009;3(12):3891–3902.
29. Wang Y, Wan J, Miron RJ, et al. Antibacterial properties and mechanisms of gold-silver nanocages. *Nanoscale.* 2016;8(21):11143–11152.
30. Chernousova S, Epple M. Silver as antibacterial agent: ion, nanoparticle, and metal. *Angew Chem Int Ed Engl.* 2013;52(6):1636–1653.
31. Li Q, Lu F, Ye HL, et al. Silver Inlaid with Gold Nanoparticles: enhanced Antibacterial Ability Coupled with the Ability to Visualize Antibacterial Efficacy. *ACS Sustainable Chem. Eng.* 2018;6(8):9813–9821.
32. Sharma VK, Siskova KM, Zboril R, et al. Organic-coated silver nanoparticles in biological and environmental conditions: fate, stability and toxicity. *Adv Colloid Interface Sci.* 2014;204:15–34.
33. Parsell DA, Lindquist S. The function of heat-shock proteins in stress tolerance: degradation and reactivation of damaged proteins. *Annu Rev Genet.* 1993;27:437–496.

34. de Oliveira NEM, Abranches J, Gaca AO, et al. clpB, a class III heat-shock gene regulated by CtsR, is involved in thermotolerance and virulence of *Enterococcus faecalis*. *Microbiology (Reading)*. 2011;157(Pt 3):656–665.
35. Doyle SM, Hoskins JR, Wickner S. Collaboration between the ClpB AAA+ remodeling protein and the DnaK chaperone system. *Proc Natl Acad Sci U S A*. 2007;104(27):11138–11144.
36. Hoskins JR, Doyle SM, Wickner S. Coupling ATP utilization to protein remodeling by ClpB, a hexameric AAA+ protein. *Proc Natl Acad Sci U S A*. 2009;106(52):22233–22238.
37. Murray BE. The life and times of the *Enterococcus*. *Clin Microbiol Rev*. 1990;3(1):46–65.
38. Soukos NS, Chen PS, Morris JT, et al. Photodynamic therapy for endodontic disinfection. *J Endod*. 2006;32(10):979–984.
39. Dong H, Cronan JE. Temperature regulation of membrane composition in the Firmicute, *Enterococcus faecalis*, parallels that of *Escherichia coli*. *Environ Microbiol*. 2021;23(5):2683–2691.
40. Radka CD, Rock CO. Mining Fatty Acid Biosynthesis for New Antimicrobials. *Annu Rev Microbiol*. 2022;76:281–304.
41. Bartolo A, Koyess E, Camilleri J, et al. Model assessing thermal changes during high temperature root canal irrigation. *Health Technol Lett*. 2016;3(3):247–251.
42. Gambarini G, De Luca M, Gerosa R. Chemical stability of heated sodium hypochlorite endodontic irrigants. *J Endod*. 1998;24(6):432–434.
43. Liu H, Nio S, Shen Y. Sodium hypochlorite against *Enterococcus faecalis* biofilm in dentinal tubules: effect of concentration, temperature, and exposure time. *Odontology*. 2023.
44. Cen R, Wang R, Cheung GSP. Periodontal Blood Flow Protects the Alveolar Bone from Thermal Injury during Thermoplasticized Obturation: a Finite Element Analysis Study. *J Endod*. 2018;44(1):139–144.

International Journal of Nanomedicine

Dovepress

## Publish your work in this journal

The International Journal of Nanomedicine is an international, peer-reviewed journal focusing on the application of nanotechnology in diagnostics, therapeutics, and drug delivery systems throughout the biomedical field. This journal is indexed on PubMed Central, MedLine, CAS, SciSearch®, Current Contents®/Clinical Medicine, Journal Citation Reports/Science Edition, EMBase, Scopus and the Elsevier Bibliographic databases. The manuscript management system is completely online and includes a very quick and fair peer-review system, which is all easy to use. Visit <http://www.dovepress.com/testimonials.php> to read real quotes from published authors.

Submit your manuscript here: <https://www.dovepress.com/international-journal-of-nanomedicine-journal>